Title

Dinuclear PhotoCORMs: Dioxygen-Assisted Carbon Monoxide Uncaging from Long-Wavelength-Absorbing Metal–Metal-Bonded Carbonyl Complexes

Journal

Inorganic Chemistry, 56(11)

ISSN

0020-1669

Authors

Li, Zhi
Pierri, Agustin E
Huang, Po-Ju
et al.

Publication Date

2017-06-05

DOI

10.1021/acs.inorgchem.6b03138

Peer reviewed

Inorganic Chemistry

Article

pubs.acs.org/IC

Dinuclear PhotoCORMs: Dioxygen-Assisted Carbon Monoxide Uncaging from Long-Wavelength-Absorbing Metal−Metal-Bonded Carbonyl Complexes

Zhi Li,[†] Agustin E. Pierri,[†] Po-Ju Huang,[†] Guang Wu,[†] Alexei V. Iretskii,[†,‡] and Peter C. Ford*[,†]

[†]Department of Chemistry and Biochemistry, University of California, Santa Barbara, Santa Barbara, California 93106-9510, United States

[‡]Department of Chemistry and Environmental Sciences, Lake Superior State University, Sault Sainte Marie, Michigan 49783, United States

Supporting Information

ABSTRACT: We describe a new strategy for triggering the photochemical release of caged carbon monoxide (CO) in aerobic media using long-wavelength visible and near-infrared (NIR) light. The dinuclear rhenium−manganese carbonyl complexes $(CO)_5ReMn(CO)_3(L)$, where L = phenanthroline (**1**), bipyridine (**2**), biquinoline (**3**), or phenanthrolinecarboxaldehyde (**4**), each show a strong metal−metal-bond-to-ligand ($\sigma_{MM} \rightarrow \pi_L^*$) charge-transfer absorption band at longer wavelengths. Photolysis with deep-red (**1** and **2**) or NIR (**3** and **4**) light leads to homolytic cleavage of the Re−Mn bonds to give mononuclear metal radicals. In the absence of trapping agents, these radicals primarily recombine to reform dinuclear complexes. In oxygenated media, however, the radicals react with dioxygen to form species much more labile toward CO release via secondary thermal and/or photochemical reactions. Conjugation of **4**, with an amine-terminated poly(ethylene glycol) oligomer, gives a water-soluble derivative with similar photochemistry. In this context, we discuss the potential applications of these dinuclear complexes as visible/NIR-light-photoactivated CO-releasing moieties (photoCORMs).

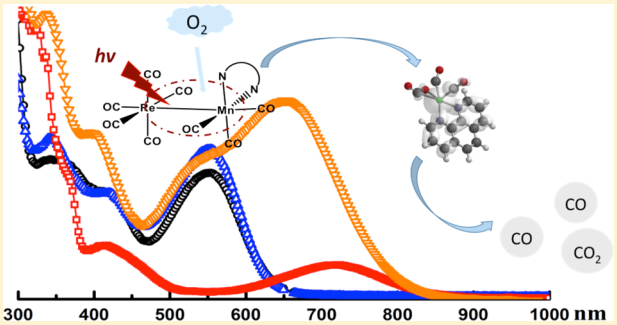

INTRODUCTION

Although carbon monoxide (CO) is an environmental pollutant categorized as dangerous to health,[1] it has long been known that CO is produced endogenously in humans by heme oxygenases.[2,3] Furthermore, CO is identified as a signaling molecule that plays roles in the suppression of inflammation, in vasorelaxation, and in wound healing.[3−10] From a medical perspective, the exogenous application of CO is linked to reduced organ graft rejection,[11] protection against ischemia/reperfusion injury,[12] and antibacterial activity.[13−16] Thus, CO joins nitric oxide and hydrogen sulfide as endogenously generated small-molecule bioregulators for which the targeted delivery may have therapeutic value.[17]

The mammalian toxicity of CO can be attributed to the inactivation of dioxygen (O_2) transport via strong CO binding with hemoglobin (Hb), although it is notable that Hb(CO) levels can reach ∼20% in the blood with limited adverse affect.[4] CO also inhibits mitochondria respiration by binding heme-containing proteins such as cytochrome *c* oxidase.[18] In this context, Hb's affinity for CO serves as a buffer against more toxic effects at the cellular level.[4] The same buffering function also affects the potential delivery of CO for investigating beneficial effects and/or therapeutic potential. Thus, it is necessary to develop methods for targeted CO delivery to physiological sites that can avoid the Hb pool in the bloodstream.

This issue has been addressed by using CO-releasing moieties (CORMs), many of which are metal carbonyl complexes that react thermally to release CO under physiological conditions.[3,19−24] Another approach is to use biocompatible compounds that are stable in aerobic media and that uncage (release) CO when activated by light as an external stimulus.[25−37] The latter we have dubbed "photoCORMs",[26] and this use of light offers exquisite spatial control of the timing and dosage of such a release. However, a major point that needs to be addressed is concerned with the wavelength of light utilized in most such systems to facilitate CO uncaging. The short-wavelength, high-energy light needed to activate most metal carbonyl complexes toward CO labilization has shallow penetration depths into mammalian tissue and can damage living cells.[38] A similar problem is encountered with organic photoCORMs, although several recent examples have extended the photosensitivity to much longer wavelengths.[39,40] Thus, there is considerable interest in developing photochemical delivery systems that can be activated with more deeply

Received: December 28, 2016
Published: March 5, 2017

DOI: 10.1021/acs.inorgchem.6b03138
Inorg. Chem. 2017, 56, 6094−6104

penetrating, longer-wavelength visible/near-infrared (NIR) light for the delivery of CO[34,41] and of other small-molecule bioregulators in aerobic media.[42,43]

There are several approaches to making photoCORM systems more responsive to longer wavelengths. Previously, this laboratory described carriers incorporating upconverting nanoparticles that used multiphoton excitation with NIR light to trigger CO release from a manganese(I) carbonyl.[34] A different strategy is described here, where we utilize direct excitation of the long-wavelength-absorbing metal−metal-bond-to-ligand charge-transfer (MMLCT)[44,45] transition of dinuclear complexes to generate reactive intermediates (proCORMs)[26] that, upon subsequent reaction(s), release CO. Specifically, MMLCT excitation of the dinuclear rhenium−manganese carbonyl complexes $(CO)_5ReMn(CO)_3(L)$ [L = 1,10-phenanthroline (phen, **1**), 2,2′-bipyridine (bpy, **2**), 2,2′-biquinoline (biq, **3**), and 1,10-phenanthroline-4-carboxaldehyde (phen-CHO, **4**)] leads to homolytic cleavage of the Re−Mn bond to give mononuclear metal radicals. In an aerobic solution, these radicals react with O_2[46] to form new species that are much more labile toward CO release (uncaging). To our knowledge, this is the first photochemical study of such dinuclear photoCORMs in aerated media to demonstrate the release of caged CO with long-wavelength excitation.

RESULTS AND DISCUSSION

Synthesis and Characterization of Dinuclear Complexes. Scheme 1 outlines the pathways used to prepare the dinuclear complexes $(CO)_5ReMn(CO)_3L$ (L = bpy, phen, biq, or phen-CHO) from the reaction of $BrMn(CO)_3L$ with $Na[Re(CO)_5]$ in anhydrous tetrahydrofuran. During the reaction, the solution color changes from pale orange to an intense violet, blue, or green, indicating the formation of dinuclear complexes. After column chromatography, product yields generally exceeded 50%. The mechanism of M−M′ bond formation in such reactions has been the subject of some debate.[47−51] On the basis of earlier work,[47] Morse and Wrighton[48] proposed electron transfer leading to two metal radicals, one a 17 e^- complex and the other a 19 e^- complex. The M−M′ bond is formed by radical coupling after halide loss from the latter intermediate. Consistent with this pathway was the isolation of $M_2(CO)_{10}$ and $M'_2(CO)_6L_2$ coproducts in addition to the desired heteronuclear complex $M(CO)_5M'(CO)_3L$. The observation that heteronuclear product yields are often quite high was explained by Tyler and coworkers[50,51] in terms of the solvent structure inhibiting escape of the heteronuclear radical pair generated by electron transfer, thereby favoring formation of the M−M′ bond. In the present case, chromatography of the crude product indicated minor byproducts that may be the result of some homonuclear coupling.

Scheme 1. Steps Leading to the Syntheses of Complexes 1−4[a]

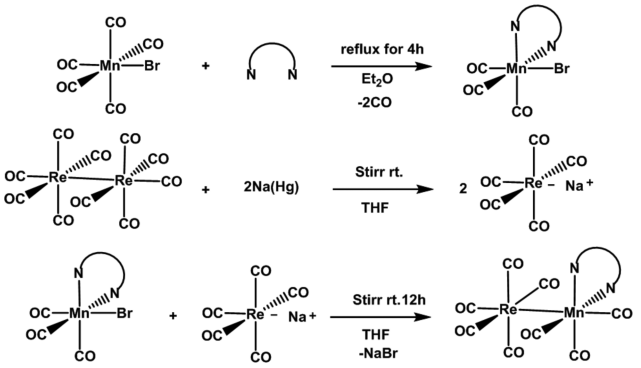

[a]The bidentate ligands are phen, bpy, biq, and phen-CHO, respectively.

Recrystallization of the heterodinuclear products gave single crystals suitable for X-ray diffraction studies (see the Supporting Information (SI), Table S1, for crystal data). Crystals of **2** are simple orthorhombic, while those of **1**, **3**, and **4** are triclinic. The structures determined from these studies are shown in Figures 1−4. The bond lengths and angles are summarized in the SI, Table S2. For each complex, the three carbonyls on the manganese are in the *facial* configuration. The bpy and phen ligands are coplanar with the coordinating manganese; however, the structure of **3** shows the plane of biq bending toward the metal−metal bond, perhaps to relieve steric crowding. Notably, the Re−Mn bond length in **3** (3.066 Å) is somewhat longer than those in **1**, **2**, and **4** at 3.005 Å (ave), 3.020 Å (ave), and 2.998 Å, respectively.

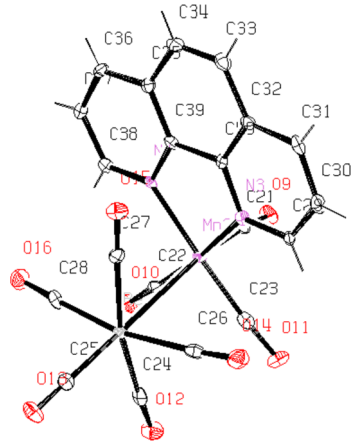

Figure 1. ORTEP drawing of the X-ray structure of **1** (with 50% thermal ellipsoids; the unit cell includes two independent molecules; see the SI, Figure S1).

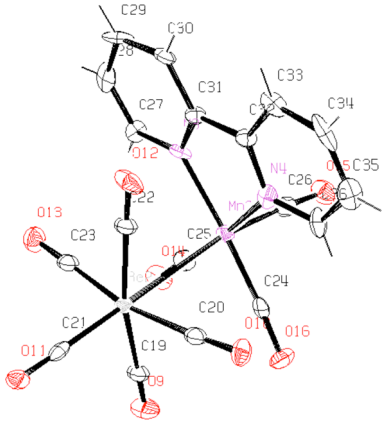

Figure 2. ORTEP drawing of the X-ray structure of **2** (with 50% thermal ellipsoids; the unit cell includes three independent molecules; see the SI, Figure S2).

DOI: 10.1021/acs.inorgchem.6b03138
Inorg. Chem. 2017, 56, 6094−6104

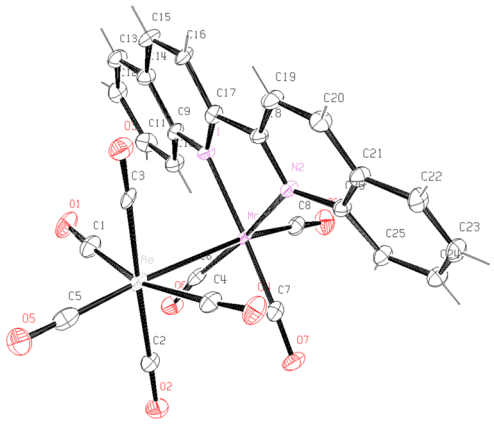

Figure 3. ORTEP drawing of the X-ray structure of **3** (with 50% thermal ellipsoids).

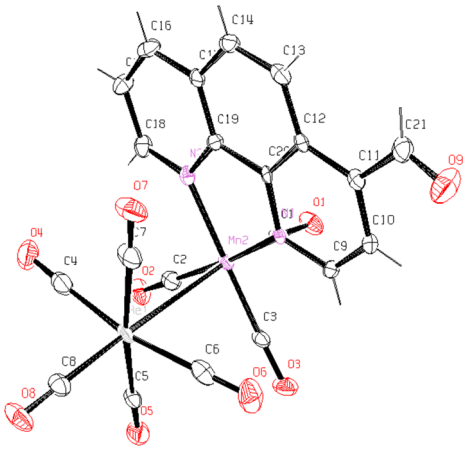

Figure 4. ORTEP drawing of **4** (with 50% thermal ellipsoids; the unit cell includes one molecule and one disordered CH_2Cl_2).

The dinuclear complexes were further characterized by recording their UV−vis, IR, NMR, and mass spectra (MS) (Figure 5 and the SI, Table S3 and Figures S3−S5). As shown in Figure 5, the visible spectrum of each in an acetonitrile

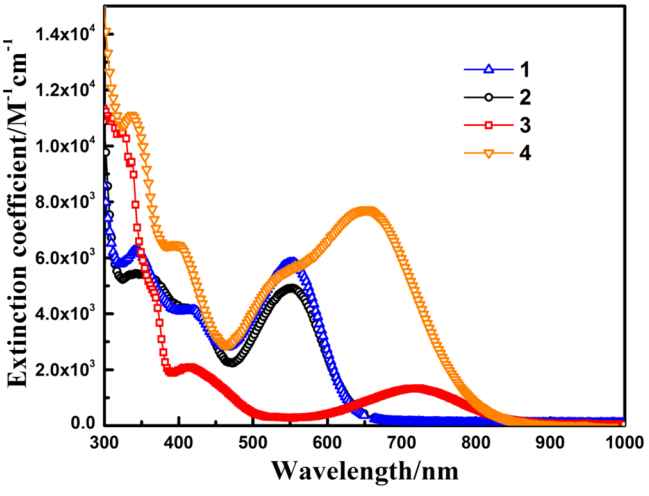

Figure 5. Visible absorption spectra of complexes **1**−**4** in ambient-temperature, aerobic MeCN showing strong MMLCT absorption bands. The respective MMLCT λ_{max} extinction coefficients are 5.8 × 10^3, 4.9 × 10^3, 1.3 × 10^3, and 7.6 × 10^3 M^{-1} cm^{-1}.

(MeCN) solution displays a strong, longer-wavelength absorption band that is sensitive to the nature of L. This band is attributed to a MMLCT ($\sigma_{MM} \rightarrow \pi_L^*$) transition in analogy to earlier studies with related complexes.[45,52] Figure S6 in the SI is a qualitative MO diagram indicating the orbital origin for such transitions. The shorter-wavelength bands in the electronic spectra include contributions from $\sigma_{MM}^{b} \rightarrow \sigma_{MM}^*$ (localized on the M−M bond), $d_\pi \rightarrow \pi_L^*$ (metal-to-ligand charge transfer), and $\pi_L \rightarrow \pi_L^*$ (intraligand) transitions. For the analogous $(CO)_5ReMn(CO)_3L$ complexes, the MMLCT band displays λ_{max} values of 550, 550, 719, and 652 nm for L = phen (**1**), bpy (**2**), biq (**3**), and phen-CHO (**4**), respectively.

Aerobic MeCN solutions of **1**, **2**, and **4** show good stability at 37 °C when kept in the dark. This was evidenced by very small (≤6%) changes of the MMLCT absorbance of **1** and **2** over a 16 h period and less than a 20% change in **4** over a 12 h period in either an aerobic or an anaerobic solution (for example, see Figure 6). In contrast, an aerated MeCN solution of the biq

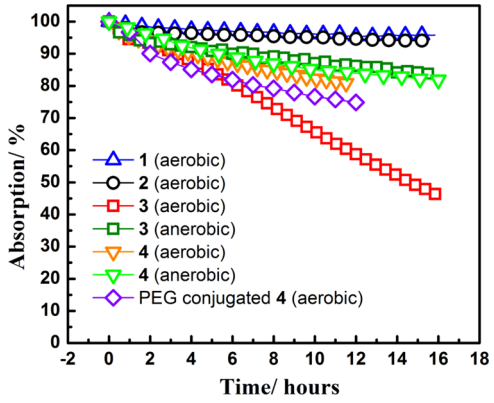

Figure 6. Normalized absorbance at λ_{max} for the MMLCT band of aerobic **1** (blue triangles), aerobic **2** (black circles), aerobic **3** (red rectangles), anaerobic **3** (olive rectangles), aerobic **4** (orange triangles), and anaerobic **4** (green triangles) in MeCN at ∼37 °C over the course of 12−16 h. Purple diamonds: Normalized absorbance at λ_{max} for the MMLCT band of PEG-conjugated **4** in an aerobic pH 7.4 PBS solution over the course of 12 h.

complex **3** proved to be less stable, with the absorbance at the MMLCT λ_{max} decreasing about 50% over a 16 h time period at 37 °C. In an anaerobic solution, however, the change is smaller (19%) over the same time period. This instability may be the result of the extra crowding from the sterically more bulky biq ligand, a feature that was also reflected in the longer Re−Mn bond.

Photochemical Studies of $(CO)_5ReMn(CO)_3$(phen) (1). The initial photochemical experiments largely focused on the phen complex **1**. The MMLCT band (λ_{max} = 550 nm) of **1** tails to longer wavelengths, so its photochemistry could be investigated using a deep-red light-emitting diode (LED) operating at 659 nm (see the SI, Figure S7), where the extinction coefficient (ε_{659}) for **1** is 315 M^{-1} cm^{-1} in MeCN. Exhaustive 659 nm photolysis of **1** in an aerobic solution fully bleached the MMLCT band (Figure 7) as well as bands at 341 and 417 nm attributed to $\sigma_{MM} \rightarrow \sigma_{MM}^*$ and $d\pi \rightarrow \pi_L^*$ transitions. The final color of the solution was a faint yellow. When photolysis was conducted in a Schlenk cuvette[26] and the gas phase was sampled after exhaustive photolysis, gas chromatography−thermal conductivity (GC−TCD) analysis indicated the release of CO. However, owing to the lower

DOI: 10.1021/acs.inorgchem.6b03138
Inorg. Chem. 2017, 56, 6094−6104

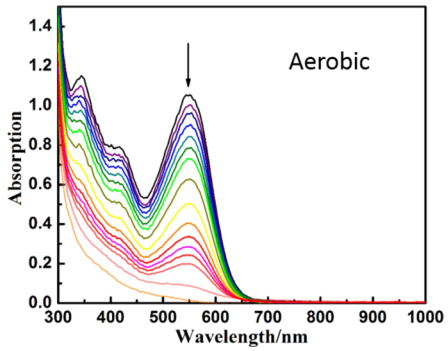

Figure 7. Absorption changes resulting from 659 nm photolysis (25 mW) of dinuclear compound **1** (1.65×10^{-4} M) in aerobic MeCN.

sensitivity of this technique, quantitative CO analysis was done with much higher concentrations (see below).

When analogous 659 nm photolysis of **1** was carried out in an anaerobic MeCN solution, the pattern of spectral changes was considerably different (Figure 8). Although the MMLCT

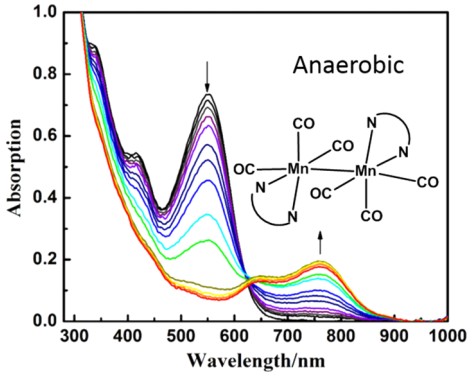

Figure 8. Optical spectral changes upon 659 nm photolysis (25 mW) of **1** (1.22×10^{-4} M) in anaerobic MeCN.

band at 550 nm disappeared, a new, longer-wavelength band appeared at ~761 nm. This observation suggests formation of the dimanganese compound $Mn_2(CO)_6(phen)_2$ (**5**) via photoinduced cleavage of the Re−Mn bond in **1**, followed by the homonuclear coupling of $Mn(CO)_3(phen)$ radicals (Scheme 2).[53,54] The 761 nm MMLCT band of the putative **5** remained unchanged under further 659 nm irradiation, suggesting that the photolytic cleavage of **5** is followed by a rapid backreaction. The other expected homonuclear coupling product $Re_2(CO)_{10}$ does not display a visible range absorbance (see the SI, Figure S8) and would not be susceptible to secondary photolysis at 659 nm. These results clearly imply that, in aerobic solutions, O_2 efficiently traps such free radicals and therefore prevents reformation of the M−M bonds.

Scheme 2. Proposed Redistribution of Dinuclear Species after MMLCT Excitation of 1 at 659 nm[a]

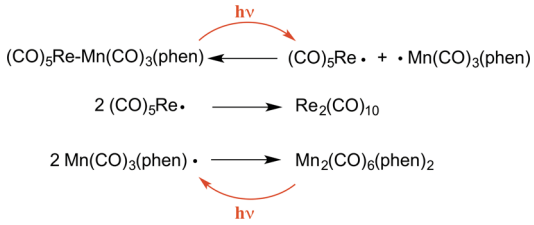

[a]The manganese dimer remains susceptible to photolysis at this λ_{irr} value, while the rhenium dimer does not absorb at this longer wavelength.

The photoproduct **5** was better characterized by examining IR spectral changes. A freeze−pump−thaw deaerated MeCN solution of **1** (4.6 mM) was transferred under argon to a KBr IR cell, which was then sealed with Teflon plugs in an inert-atmosphere glovebox. This solution was then photolyzed with the 659 nm LED, and the IR spectral changes were periodically recorded (see the SI, Figure S9a). Before photolysis, the spectrum of **1** displayed ν_{CO} bands at 1884, 1975, and 2076 cm^{-1}. During irradiation at 659 nm, new bands characteristic of $Re_2(CO)_{10}$ appeared at 1968, 2009, and 2070 cm^{-1} and remained unchanged upon further photolysis (see the SI, Figure S9b). Synchronously, two lower-frequency ν_{CO} bands appeared at 1857 and 1934 cm^{-1}, which are close to bands previously observed in 2-methyltetrahydrofuran for a species identified in situ as **5**.[51] The lower-frequency ν_{CO} bands in the homonuclear dimer relative to **1** may be attributed to rhenium having a higher electronegativity than manganese,[55] leading to polarization of the Re−Mn bond, which draws the electron density away from the manganese center in **1**. The latter two ν_{CO} bands did eventually disappear upon standing, an observation attributed to the imperfect seal of the IR cell and slow leakage of air into the system.

The assignment of **5** draws further support from the 659 nm photolysis of **1** in a deaerated CD_3CN solution in a sealed J. Young NMR tube. The ^1H NMR spectra were recorded before and after photolysis (see the SI, Figure S10) and show that the four ^1H resonances characteristic of coordinated phen for the photolyzed product are all shifted to higher field compared to the analogous peaks in the spectrum of **1**. Only one new set of phen resonances is seen, consistent with the formation of a symmetrical homonuclear dimer, and the upfield shift is consistent with greater Mn-to-phen back-bonding in this product.

In an aerobic solution, 659 nm photolysis of **1** (2.8 mM) in an IR cell gave somewhat different results. The ν_{CO} bands for **1** decreased, while those for $Re_2(CO)_{10}$ and **5** appeared, but the latter were less intense than those in an anaerobic solution (see the SI, Figure S11). Differences included broadening of the bands at ~1867 cm^{-1} and the appearance of a weak band at ~2120 cm^{-1}. Thus, under these conditions, O_2 trapping of radicals occurs but is incomplete presumably because the O_2 initially present in the sealed KBr cell (~1.7 mM)[56] is depleted in the early stages and not replenished.

Figure 9 illustrates the optical spectral changes when an analogous photolysis of **1** was carried out in deaerated 90:10 MeCN/chloroform. Similar to the experiment under aerobic conditions, the MMLCT band at 550 nm was depleted, but no bands indicating the formation of new dinuclear species were observed. These observations are consistent with Scheme 2; however, in this case, the radicals formed by photolytic cleavage of the Re−Mn bond would be trapped by $CHCl_3$ (Scheme 3).[57] The absorption bands at 417 nm decreased in intensity but did not disappear, which would be expected, because the $d\pi \rightarrow \pi_L^*$ transition of $Mn(CO)_3(phen)Cl$ is also around 420 nm.[58] Although second-order rate constants for the recombination d^7 metal carbonyl radicals are several orders of magnitude higher than those for trapping by halocarbons, the high chloroform concentration (~1.3 M) makes such trapping efficient.[57,59,60]

DOI: 10.1021/acs.inorgchem.6b03138
Inorg. Chem. 2017, 56, 6094−6104

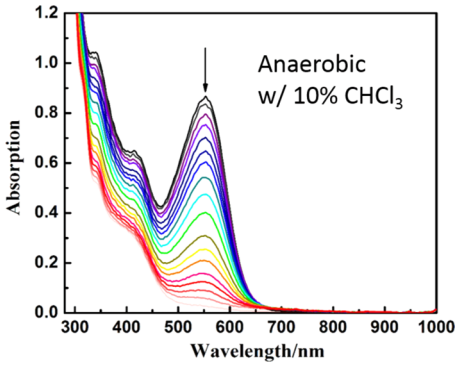

Figure 9. Absorption change upon photolysis of **1** (0.135 mM) at 659 nm (25 mW) in anaerobic 90:10 MeCN/$CHCl_3$.

Scheme 3. Photolysis of the MMLCT Band of 1 in Solutions Containing $CHCl_3$, Leading to Trapping of the Radicals Formed by Re−Mn Bond Cleavage

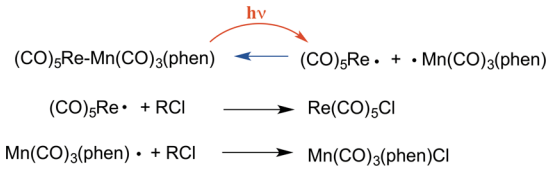

The temporal absorbance changes at the MMLCT λ_{max} upon photolysis (e.g., Figures 7−9) were used to determine the quantum yields (Φ_{MM}) for disappearance of **1**, as calculated from the slopes of the $N_{reacted}$ versus N_{abs} plots (Figure 10). The

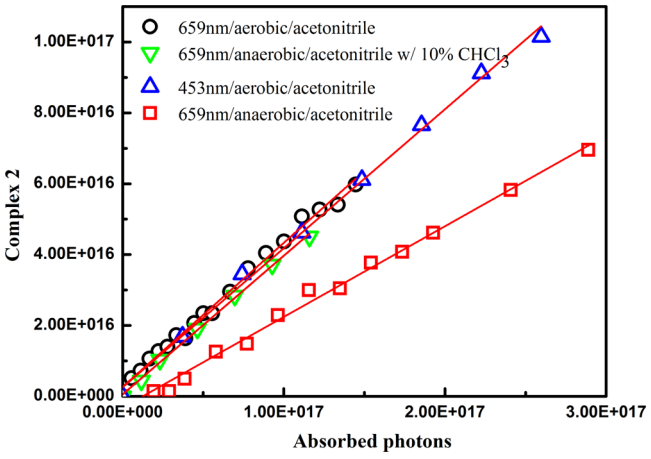

Figure 10. Quantum yield (Φ_{MM}) measurements: (black circles) 659 nm photolysis of **1** (0.165 mM) in aerobic MeCN; (green triangles) 659 nm photolysis of **1** (0.135 mM) in anaerobic 9:1 MeCN/$CHCl_3$; (red rectangles) 659 nm photolysis of **1** (0.122 mM) in anaerobic MeCN; (blue triangles) 435 nm photolysis of **1** (0.165 mM) in aerobic MeCN.

Φ_{MM} value thus determined for 659 nm photolysis of **1** in aerobic MeCN was 0.41 ± 0.01 (three independent measurements). This plot was essentially indistinguishable from that obtained for 659 nm photolysis under anaerobic conditions in 90:10 MeCN/$CHCl_3$ (Φ_{MM} = 0.39 ± 0.01). Thus, it appears that the photolysis-generated radicals were efficiently trapped, either by O_2 in an aerobic solution or by $CHCl_3$ in the latter solution (Scheme 3).

Consistent with this conclusion is Φ_{MM} (0.38 ± 0.01; see the SI, Figure S12) determined for 659 nm photolysis of **1** in MeCN saturated with pure O_2 (~8.1 mM),[56] essentially the same as that measured in an air-equilibrated solution. Notably, 453 nm photolysis in an aerobic MeCN solution also gave an equivalent value of Φ_{MM} (0.39 ± 0.01; Figure 10), suggesting that an internal conversion/intersystem crossing from the state(s) initially populated by higher-energy excitation to those responsible for M−M cleavage is very efficient. In contrast, the value determined in anaerobic MeCN (Φ_{MM} = 0.26 ± 0.01) was lower, a result that can be attributed to the radical recombination outlined in Scheme 2.

Photolyses of Complexes 2−4. Values of Φ_{MM} were also measured for 659 nm photolyses of the bpy, biq, and phen-CHO complexes in aerobic MeCN. The Φ_{MM} value for **2** was 0.39 ± 0.01 (see the SI, Figure S13), very close to that for **1** under analogous conditions, while a Φ_{MM} value of 0.24 ± 0.02 was found for the biq complex **3** (see the SI, Figure S14). In neither case was the nature of the products explored further. Surprisingly, under 659 nm photolysis, the phen-CHO complex **4** displays a much smaller Φ_{MM} value of 0.0153 ± 0.0004 (see the SI, Figure S15), although it should be noted that the extinction coefficient of **4** at this wavelength (ε_{659} = 7.7 × 10^3 M^{-1} cm^{-1}) is ~24-fold higher than that of **1**. Because the rate of the photochemical reaction is equal to $\Phi_{MM}I_a$ (where I_a is the intensity of the light *absorbed*),[43] the much larger extinction coefficient for **4** at this wavelength makes up in large part for the lower quantum yield.

The MMLCT absorption bands of both **3** and **4** extend into the NIR region, where the transmission of light through tissue is optimal. Photolysis of **4** (ε_{794} = 940 M^{-1} cm^{-1}) at 794 nm with a NIR diode laser led to complete bleaching of the MMLCT band and with a Φ_{MM} value of 0.0165 ± 0.0002 in aerobic MeCN (Figure 11). Similarly, 794 nm photolysis of **3** (ε_{794} = 646 M^{-1} cm^{-1}) gave Φ_{MM} = 0.170 ± 0.002, about 30% lower than that under 659 nm irradiation (Figure 12).

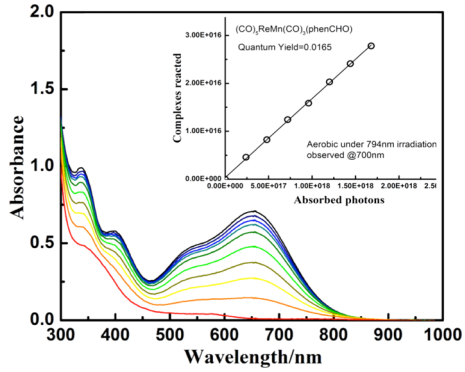

Figure 11. Optical spectral changes upon 794 nm photolysis (203 mW) of **4** (initially 9.3 × 10^{-5} M) in aerobic MeCN. ***Inset:*** Quantum yield measurement: Φ_{MM} = 0.0165.

CO Release. Table 1 summarizes the quantitative CO release measured by GC−TCD analysis of the gas phase after exhaustive photolysis of solutions of **1** in a Schlenk cuvette. As noted above, these experiments used a relatively high substrate concentration (~2.75 mM) owing to the lower sensitivity of GC−TCD analysis. The key observation is that 659 nm photolysis in an aerobic solution led to CO release in each case; however, no CO was detected when analogous photolysis was conducted either in anaerobic MeCN or in 90:10 MeCN/

DOI: 10.1021/acs.inorgchem.6b03138
Inorg. Chem. 2017, 56, 6094−6104

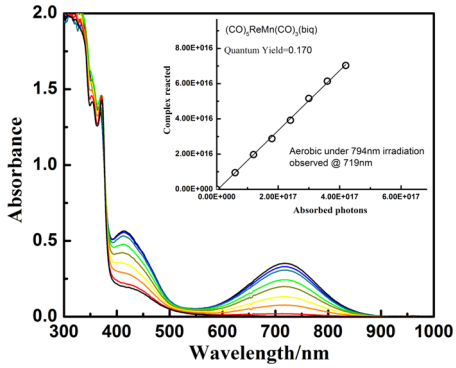

Figure 12. Optical spectral changes upon 794 nm photolysis (50 mW) of **3** (initially 2.64×10^{-4} M) in aerobic MeCN. Inset: Quantum yield measurement ($\Phi_{MM} = 0.17$).

Table 1. CO Release upon Exhaustive Photolysis of Compound 1 under Various Conditions

atmosphere	solvent(s)	λ_{irr} (nm)	CO per complex (mol mol^{-1})	CO_2 per complex (mol mol^{-1})
aerobic	MeCN	453[a]	2.28	0.52
		659[a]	2.01	0.81
		659[b]	1.96	0.78
anaerobic		659[a]	<0.09	<0.06
	90:10 MeCN/$CHCl_3$	659[a]	<0.07	<0.05
aerobic	DCM	659[a]	1.87	0.24

[a][**2**] = 2.75 mM. [b][**2**] = 0.13 mM.

$CHCl_3$. Given that the principal photoreaction pathway upon MMLCT excitation is Re−Mn bond cleavage, there is clearly a direct correlation between trapping of these radicals by O_2 and the uncaging of CO. Exhaustive photolysis with the deep-red LED in an aerobic solution led to the release of ∼2 mol of CO per 1 mol of **1** for two very different substrate concentrations (2.75 and 0.13 mM). A somewhat higher value of 2.3 mol of CO per mol of **1** was seen for photolysis with a blue LED (λ_{irr} = 453 nm; see the SI, Figure S7) in aerobic media. This may be the result of secondary photolysis Re−Mn bond cleavage products because there was residual absorbance at 453 nm after exhaustive photolysis at 659 nm. CO release was also observed for the photolysis of **1** in aerobic dichloromethane (DCM). Because CH_2Cl_2 is a much less effective radical-trapping agent than $CHCl_3$ is,[57] it is likely that O_2 trapping of the photolysis-generated radicals predominates in this case as well.

In each case, carbon dioxide (CO_2) was also generated during irradiation in an aerobic solution (Table 1). A similar observation was made when the tungsten carbonyl complex $W(CO)_5(L')^{3-}$ [L′ = tris(sulfonatophenyl)phosphine trianion] was photolyzed in an aerated aqueous solution.[26] In that case, CO_2 formation was attributed to CO oxidation by redox-active intermediates formed upon O_2 reactions with low-valent metal carbonyl centers.

Quantum yields for CO release (Φ_{CO}) in aerobic MeCN were determined with high concentrations of **1** (2.75 mM) in order to use GC−TCD analysis to measure the CO released at several time points during photolysis. The value of Φ_{CO} (0.4 ± 0.1) for irradiation at 659 nm was determined from the plot of N_{CO} (molecules of CO released) versus N_{abs} (see the SI, Figure S16). Given that, under these conditions, ∼2 mol of CO is released per 1 mol of substrate upon exhaustive photolysis, this value of Φ_{CO} is less than what might be expected. One possible explanation would be a less efficient net photolytic cleavage at this concentration, which is ∼17-fold higher than that used to determine the Φ_{MM} values reported (see above). The greater absorbance at the 659 nm λ_{irr} leads to a higher flux of transient radicals. Because the O_2 in air-saturated MeCN is <∼1.7 mM, radical recombination may play a greater role, thereby giving a lower Φ_{MM}, although exhaustive photolysis would still have the same 2:1 Φ_{CO}/Φ_{MM} ratio, owing to the reservoir of O_2 in the gas phase of the Schlenk cuvette. This argument is consistent with the IR experiment in aerobic MeCN, where 659 nm photolysis of **1** at a comparable concentration (2.75 mM) of radical recombination products was evident. Using the same method, NIR (794 nm) irradiation of **4** (2.5 mM in MeCN) gave a Φ_{CO} value of 0.015 ± 0.001 (see the SI, Figure S17), and exhaustive 794 nm photolysis of **4** led to the release of ∼1.5 mol of CO per 1 mol of substrate.

Studies in Aqueous Solution. While complexes **1**−**4** provide a proof-of-principle for using long-wavelength MMLCT excitation of dinuclear metal carbonyls to trigger photochemical CO release in aerobic media, they are not soluble in aqueous solution. In some cases, the hydrophobic nature of these complexes may be an advantage, for example, when used in a biocompatible polymer disk as an implant[61−63] or with amphiphilic polymer-base water-soluble nanocarriers[34] and micelles.[64,65] We are indeed pursuing both options with these photoCORMs. On the other hand, substituents on the phen ligands offer possible modifications to enhance the aqueous solubility.

One such substituent is the carboxaldehyde on **4**. The reaction of $(CO)_5ReMn(CO)_3$(phen-CHO) with an amine-terminated poly(ethylene glycol) (PEG) PG1-AM-2k (average mol wt = 3135 Da) gave a water-soluble conjugate linked through an imine bond (eq I). The product $(CO)_5ReMn(CO)_3$(phen-CHNPEG) (**6**) was characterized by ^{1}H NMR spectroscopy (see the SI, Figure S3e), where it was shown that the aldehyde proton disappears and the ratio between the phen ligand and PEG moiety is approximately 1:1, which confirms its structure. This material displayed a broad absorption band with a λ_{max} value of ∼569 nm and a broad shoulder at 700 nm with absorbance extending beyond 800 nm, presumably the MMLCT transition(s) (see the SI, Figure S18). In an aerobic pH 7.4 phosphate-buffered saline (PBS) solution at 37 °C, **6** demonstrated moderate stability, with absorbance at the MMLCT λ_{max} diminishing about 20% over 12 h (Figure 6).

$$(CO)_5ReMn(CO)_3(\text{phen-CHO}) + H_2N\text{-PEG} \rightarrow (CO)_5ReMn(CO)_3(\text{phen-CHNPEG}) + H_2O \quad \text{(I)}$$

NIR photolysis did demonstrate **6** to be photoactive in an aerobic pH 7.4 PBS solution, as evidenced by decreases of the MMLCT absorption (see the SI, Figure S18). However, the quantum yield measured upon irradiation of such solutions with 794 nm light from a diode laser proved to be quite modest [$\Phi_{MM} = (1.0 \pm 01) \times 10^{-3}$].

Potential Mechanisms. Neither CO nor CO_2 was observed upon MMLCT photolysis of **1** in deaerated MeCN (Table 1). This result argues that the radicals initially formed by cleaving the Re−Mn bond (Scheme 2) are not sufficiently substitution-labile to generate relevant quantities of CO before recombining (Scheme 2) or being trapped by $CHCl_3$ (Scheme 3). Thus, the CO (and CO_2) released (or formed) upon longer-wavelength excitation under aerobic conditions must

DOI: 10.1021/acs.inorgchem.6b03138
Inorg. Chem. 2017, 56, 6094−6104

Scheme 4. Proposed Mechanism of Photooxidation of Complex 1

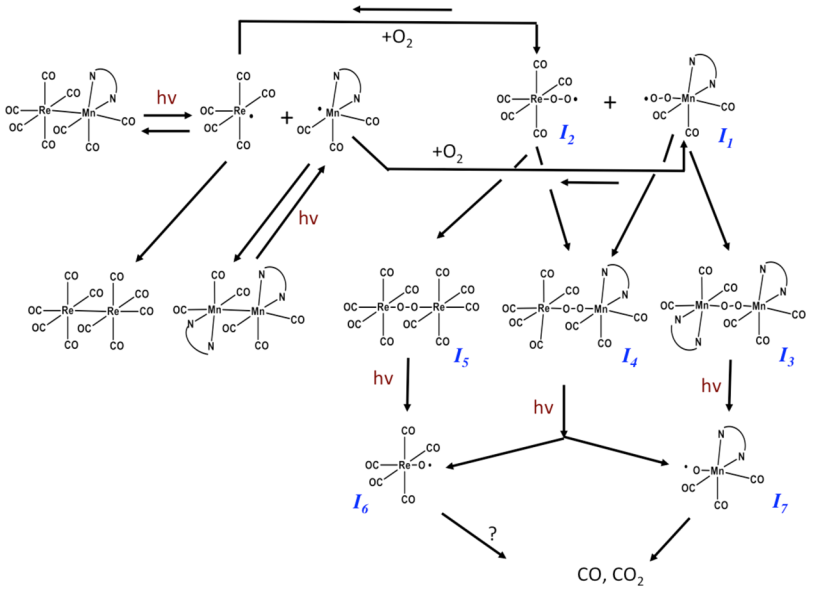

involve O_2 trapping of such metal-centered radicals. In this context, we note earlier studies that used $\sigma_{MM} \rightarrow \sigma_{MM}^*$ excitation of the complexes $M_2(CO)_{10}$ (M = Mn or Re) in 10 K Ar/O_2 matrixes and IR spectroscopy to identify the peroxo-bridged adducts $(CO)_5M(\mu\text{-}O_2)M(CO)_5$ formed presumably via eqs II and III.[46,66−68]

$$\bullet M(CO)_5 + O_2 \rightleftharpoons \bullet O_2M(CO)_5 \quad \text{(II)}$$

$$\bullet M(CO)_5 + \bullet O_2M(CO)_5 \rightleftharpoons (CO)_5M(\mu\text{-}O_2)M(CO)_5 \quad \text{(III)}$$

The mechanistic sequence proposed in Scheme 4 for the photolysis of **1** in aerobic media begins with MMLCT excitation to trigger homolytic cleavage of the Re−Mn linkage. The resulting rhenium and manganese radicals can recouple in several ways (Scheme 2) or be trapped by O_2 to form the intermediates $\bullet O_2Mn(CO)_3(phen)$ ($\mathbf{I_1}$) and $O_2Re(CO)_5$ ($\mathbf{I_2}$). Density functional theory (DFT) studies show the latter reactions to be exothermic by −15 and −21 kcal mol^{-1}, respectively (see the SI, Table S4). Furthermore, spin density analysis indicates that, while the unpaired electrons of $\bullet Mn(CO)_3(phen)$ and $\bullet Re(CO)_5$ are largely localized on the respective metal centers (see the SI, Figure S19a,b), the unpaired electrons of the O_2 adducts are largely localized on the respective O_2 ligands (see the SI, Figure S19c,d). Thus, these are superoxide complexes of the metal(I) centers and should be very reactive with subsequently generated metal-centered radicals to give the peroxo-bridged species $\{Mn(CO)_3(phen)\}_2(\mu\text{-}O_2)$ ($\mathbf{I_3}$), $(CO)_5Re(\mu\text{-}O_2)Mn(CO)_3(phen)$ ($\mathbf{I_4}$), and $[(CO)_5Re]_2(\mu\text{-}O_2)$ ($\mathbf{I_5}$). The DFT studies show that all such reactions are exothermic (see the SI, Table S4, and Figure 13).

The peroxo-bridged dirhenium complex $\mathbf{I_5}$ was identified in the IR study noted above[46] as the product of broad-band photolysis of $Re_2(CO)_{10}$ in 10 K Ar/O_2 matrixes. The same study found that continued broad-band photolysis gave a second intermediate suggested to be $ORe(CO)_5$ ($\mathbf{I_6}$), with the eventual products being Re_2O_7, CO, and CO_2.

Because $\mathbf{I_1}$−$\mathbf{I_5}$ are all formally low-spin metal(I) d^6 complexes, one would also not expect any of these to be very

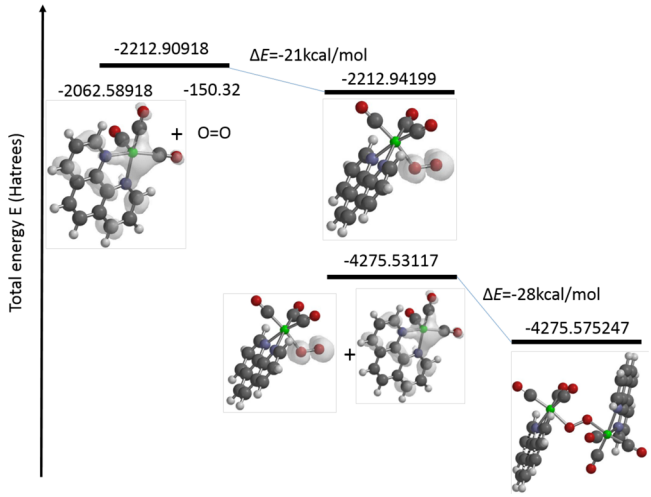

Figure 13. Total energies (E) of the intermediates $Mn(CO)_3(phen)$, $\mathbf{I_1}$, and $\mathbf{I_3}$ calculated by DFT at an unrestricted B3LYP/6-31G* level of theory without symmetry constraints.

labile toward CO release. So, the question remains, what pathway is responsible for this labilization? The DFT calculations provide some further insight into this question (see the SI, Table S4). For example, the O−O bonds of the peroxo-bridged dinuclear complexes $\mathbf{I_3}$, $\mathbf{I_4}$, and $\mathbf{I_5}$ are relatively weak with calculated bond dissociation energies of 35, 50, and 43 kcal mol^{-1}, respectively, for spontaneous dissociation to form the doublet mononuclear oxo complexes (eq IV). Thermal reactions leading to the latter species are accessible, although not likely to be fast, and certainly would not have played a role in the low-temperature matrix studies with $Re_2(CO)_{10}$ noted above. However, as indicated in that study, this process may also be activated photochemically. In this context, it is notable that time-dependent DFT (TDDFT) calculations predict that the spectra of all three peroxo-bridged intermediates should display long-wavelength visible or NIR transitions involving charge transfer from a (mostly O−O bonding) highest occupied molecular orbital (HOMO; or HOMO−1) to lowest unoccupied molecular orbitals

DOI: 10.1021/acs.inorgchem.6b03138
Inorg. Chem. 2017, 56, 6094−6104

(LUMOs) largely localized on a phen, or with $\mathbf{I}_5$, delocalized on carbonyls (see the SI, Figure S20). The resulting excited states should be more labile to homolytic O−O bond cleavage.

$$(ML_5)_2(\mu\text{-}O_2) \rightleftharpoons 2\,^2[OML_5] \quad \text{(IV)}$$

Cleavage of the peroxo bonds of $\mathbf{I}_3$, $\mathbf{I}_4$, or $\mathbf{I}_5$ would lead initially to the doublet state oxo radical intermediates ^{2}[ORe(CO)$_5$] ($^2\mathbf{I}_6$) and ^{2}[OMn(CO)$_3$(phen)] ($^2\mathbf{I}_7$). In each case, the unpaired spin is largely localized on the oxo ligand (see the SI, Figure S19e,f). Notably, for the rhenium intermediate, the doublet (or low-spin form) $^2\mathbf{I}_6$ is the lowest-energy state, with the corresponding sextet high-spin form dramatically higher in energy, as expected for a third-row transition metal (see the SI, Table S4). In contrast, for the manganese analogue, the sextet is the lower-energy state, with $^6\mathbf{I}_7$ having a calculated energy 6 kcal mol^{-1} lower than that of $^2\mathbf{I}_7$. Furthermore, the calculated structure of the high-spin state is highly distorted, showing the oxo ligand to have moved toward the carbon of an adjacent carbonyl as if to form CO_2 spontaneously and the remaining Mn−CO bonds bent significantly from linear to suggest weakening of the metal carbonyl bonding (see the SI, Figure S19g). Thus, $^6\mathbf{I}_7$ is primed for the release of two CO groups and the formation of CO_2. While there are undoubtedly other mechanisms both for CO release and for CO_2 formation in this complicated system, it is notable that long-wavelength photolysis of **1** in aerobic media generally releases two CO groups per complex and nearly one CO_2, as predicted by the calculations.

In summary, by exploiting metal−metal bond labilization upon MMLCT excitation of dinuclear rhenium−manganese carbonyls in aerobic media, we have developed a new strategy for photouncaging CO by long-wavelength red or NIR light. For complex **1**, deep-red excitation of the $\sigma_{MM} \rightarrow \pi_L^*$ transition leads to homolytic cleavage of the Re−Mn bond. O_2 trapping of the resulting Mn(CO)$_3$(phen) radical results eventually in the release of two CO groups and the apparent oxidation of one to CO_2. By rational ligand modification, the MMLCT absorption bands can be extended to the NIR (e.g., compounds **3** and **4**), where photochemical reactivity and CO uncaging are seen with 794 nm excitation. Although the Φ_{CO} values determined at this excitation wavelength are modest, the phen-CHO complex **4** illustrates the potential for further functionalization. Not only is this compound photoactive at NIR wavelengths, but it also can be conjugated to an amine-terminated PEG oligomer to give a water-soluble derivative. Continuing studies are directed along several related pathways. The most obvious will be to explore the use of hydrophobic versions of these dinuclear complexes with biocompatible polymer matrixes as their drug-delivery systems in the form of nano/microcarriers or as implantable disks. A second will be to exploit ligand modifications to enhance aqueous solubility and/or to attach targeting molecules such as certain peptide oligomers[69] to provide spatiotemporal control of CO delivery to specific cellular types or tissues.

EXPERIMENTAL SECTION

Materials. Manganese pentacarbonyl bromide (98%), dirhenium decacarbonyl (98%), and anhydrous 1,10-phenanthroline (phen) were purchased from Strem Chemicals and used without further purification. The ligands 2,2′-bipyridine (bpy; 99%) and 2,2′-biquinoline (biq; 98%) were purchased from Aldrich Chemicals. The amine-terminated poly(ethylene glycol) (PEG) PG1-AM-2k was purchased from NANOCS (average mol wt = 3135 Da).

Analytical Instrumentation. Solution optical absorption spectra were recorded in 1.0-cm-path-length quartz cells using Shimadzu dual-beam UV-2401 PC and StellarNet SL5-DH spectrophotometers. IR spectra of solutions were recorded using a Mattson Research Series FTIR spectrometer. Solution NMR spectra were recorded using a Varian Unity Inova 500 MHz spectrometer. Exact molecular masses were measured using a Waters (Milford, MA) GCT Premier time-of-flight mass spectrometer with field desorption (FD) ion sources. CO release was quantified using an Agilent 6890 gas chromatograph with a thermal conductivity detector.

Syntheses. The precursors *fac*-Mn(CO)$_3$(bpy)Br, *fac*-Mn(CO)$_3$(phen)Br, phen-CHO, fac-Mn(CO)$_3$(phen-CHO)Br, and Na[Re(CO)$_5$] were prepared by procedures described in the SI. The NMR spectra of compounds **1**−**5** are displayed with assignments in the SI and Figure 3a−e. Detailed UV−vis and IR absorption spectra for compounds **1**−**4** are tabulated in the SI, Table S3a,b.

*(CO)$_5$ReMn(CO)$_3$(phen) (**1**).* This was prepared by a modification of published procedures.[70,71] The tetrahydrofuran (THF) solution containing the rhenium salt Na[Re(CO)$_5$] (1.33 mmol) was transferred via cannula to a round-bottom flask containing Mn(bpy)(CO)$_3$Br (0.5 g, 1.33 mmol) dissolved in 25 mL dry THF. The color changed immediately from yellow to very dark purple. The mixed solution was then allowed to stir under argon in the dark. After 12 h, the solvent was removed under vacuum, and the resulting purple solid was purified by flash chromatography over activated alumina. The column was washed with one column volume of pure hexanes, and then the product mixture was eluted with a gradient of dichloromethane (DCM)/hexanes (0−50% DCM). The purple band was collected and further purified by recrystallization from DCM by slow vacuum evaporation of the solvent. The total yield was determined to be 63%. ^{1}H NMR (500 MHz, ((CD$_3$)$_2$CO, ppm): δ 9.75 (d, J(H,H) = 6.3 Hz, 2H), 8.69 (dd, J(H,H) = 8.0 and 1.1 Hz, 2H), 8.25 (s, 2H), 8.03 (dd, J(H,H) = 8.0 and 5.3 Hz, 2H) (see the SI, Figure S3a). Elem anal. Found: C, 37.20; H, 1.23; N, 4.34. Calcd: C, 37.21; H, 1.23; N, 4.34. FD + MS: m/z 645.88. Calcd: m/z 645.92.

*(CO)$_5$ReMn(CO)$_3$(bpy) (**2**).* The synthesis and purification procedures were analogous to those for **1**. The total yield was determined to be 62%. ^{1}H NMR (500 MHz, CD$_3$CN, ppm): δ 9.30 (d, J(H,H) = 5.4 Hz, 2H), 8.44 (d, J(H,H) = 8.2 Hz, 2H), 7.94 (td, J(H,H) = 8.2 and 1.4 Hz, 2H), 7.44 (ddd, J(H,H) = 7.1, 5.8, and 1.2 Hz, 2H) (see the SI, Figure S3b). Elem anal. Found: C, 34.56; H, 1.26; N, 4.49. Calcd: C, 34.79; H, 1.30; N, 4.51. FD + MS: m/z 621.87. Calcd: m/z 621.92.

*(CO)$_5$ReMn(CO)$_3$(biq) (**3**).* The synthesis and purification procedures were analogous to those for **1**. The total yield was determined to be 33.0%. ^{1}H NMR (500 MHz, CD$_3$CN, ppm): δ 8.84 (d, J(H,H) = 8.6 Hz, 2H), 8.47 (d, J(H,H) = 8.6 Hz, 2H), 8.19 (d, J(H,H) = 8.5 Hz, 2H), 8.0 (d, J(H,H) = 8.1 Hz, 2H), 7.82 (ddd, J(H,H) = 8.4, 6.9, and 1.4 Hz, 2H), 7.65 (ddd, J(H,H) = 8.1, 6.9, and 1.2 Hz, 2H) (see the SI, Figure S3c). Elem anal. Found: C, 43.43; H, 1.63; N, 4.02. Calcd: C, 43.28; H, 1.68; N, 3.88. FD + MS: m/z 721.89. Calcd: m/z 721.95.

*(CO)$_5$ReMn(CO)$_3$(phen-CHO) (**4**).* The synthesis and purification procedures were analogous to those for **1**. A total of 60 mL of a THF solution containing the rhenium anion NaRe(CO)$_5$ (2.21 mmol) was transferred via cannula to another round-bottom flask containing Mn(CO)$_3$(phen-CHO)Br (0.8 g, 1.87 mmol) dissolved in 30 mL of dry THF. The mixed solution was then allowed to stir overnight under argon, with exclusion of light. The color change from magenta to dark blue should be seen after the addition. After the solution was allowed to stand overnight, the solvent was removed under vacuum, and the resulting blue solid was purified by flash chromatography over activated alumina. The column was washed with one column volume of pure hexanes, and then the product mixture was eluted with a gradient of DCM/hexanes (0−50% DCM). The blue band was collected and further purified by recrystallization from DCM by slow vacuum evaporation of the solvent. The total yield was determined to be 0.22 g (23%). ^{1}H NMR (500 MHz, CDCl$_3$, ppm): δ 10.60 (s, 1H), 9.96 (d, J(H,H) = 5.6 Hz, 1H), 9.72 (dd, J(H,H) = 5.4 and 1.1 Hz, 1H), 9.21 (d, J(H,H) = 9.2, 1H), 8.37 (dd, J(H,H) = 8.0 and 1.1 Hz, 1H), 8.14 (d, J(H,H) = 9.2 Hz, 1H), 7.95 (d, J(H,H) = 5.6 Hz, 1H), 7.78 (dd, J(H,H) = 7.9 and 5.4 Hz, 1H) (see the SI, Figure S3d). Elem

DOI: 10.1021/acs.inorgchem.6b03138
Inorg. Chem. 2017, 56, 6094−6104

anal. Found: C, 37.66; H, 1.36; N, 3.79. Calcd: C, 37.45; H, 1.20; N, 4.16. FD + MS: *m/z* 673.87. Calcd: *m/z* 673.92.

Synthesis of an Imine PEG Conjugate (5). In a glovebox, 88 mg (0.13 mmol) of $(CO)_5ReMn(CO)_3$(phen-CHO) and 234 mg of PG1-AM-2k (amino PEG) were added to anhydrous ethanol. To the resulting solution was added 4 g of activated 3 Å molecular sieves, and then the solution was stirred at ambient temperature under an argon atmosphere with exclusion of light. The course of the reaction was monitored by thin-layer chromatography (TLC) and stopped after ~12 h. Molecular sieves and their residue were filtered, and the solvent was removed under vacuum. The resulting blue powder was purified by flash chromatography over neutral alumina with 1:1 (v/v) methanol/DCM, and the blue band was collected according to TLC. The total yield was determined to be 60 mg (19%). ^{1}H NMR (500 MHz, $CDCl_3$, ppm): δ 9.72 (d, J(H,H) = 5.6 Hz, 1H), 9.69 (d, J(H,H) = 5.3 Hz, 1H), 9.02 (s, 1H), 8.93 (d, J(H,H) = 9.2 Hz, 1H), 8.31 (dd, J(H,H) = 8.0 and 1.1 Hz, 1H), 8.03 (d, J(H,H) = 7.6 Hz, 1H), 8.01 (d, J(H,H) = 4.2 Hz, 1H), 7.72 (dd, J(H,H) = 8.0 and 5.4 Hz, 1H), 3.64 (m, 284H), 3.38 (s, 3H) (see the SI, Figure S3e).

X-ray Crystallography. The solid-state crystal structures of **1**−**4** were determined by X-ray diffraction on a Kappa Apex II single-crystal diffractometer. The X-ray structural data are summarized in the SI, Table S1.

Photochemical Studies. Photolysis experiments were carried out using 453 and 659 nm LEDs from LUXEON Rebel with total power of ~500 and 350 mW, respectively, and their emission spectra are shown in the SI, Figure S7. Photoexcitation at 794 nm was accomplished with a Sheaupac NIR fiber-coupled laser module with a laser-diode controller and laser-diode temperature controller from ILX Lightwave with a custom-built Peltier thermoelectric-cooled laser-diode module. Incident photon flux during photolysis was measured using Newport optical power/energy meter model 8442 PE with a silicon photodiode model 884-UVR detector. The irradiation time was controlled by a shutter drive/timer UniBlitz model SD-1000.

The photolysis solutions were contained in a custom-made Schlenk cuvette consisting of a 1.0-cm-path-length cuvette fused to glass tubing and stopcocks designed for attachment to a vacuum line for degassing or introducing a specific gas. This apparatus has a port sealed by a septum, through which gas samples are withdrawn using a gastight syringe for GC−TCD analysis. An analogous Schlenk cuvette is shown in the Supporting Information of ref 26. Solutions for anaerobic experiments were degassed by repetitive (three times) freeze−pump−thaw procedures, after which the Schlenk cuvette was backfilled with purified argon. After photolysis, the gas phase was sampled by drawing out an aliquot with a gastight syringe and analyzing it by GC−TCD. The total amount of CO released during photolysis was then calculated by taking into account the cell volume, solution volume, and CO solubility in the solvent, from which was determined the partitioning between the gas and liquid.

Quantum yield measurements used the power meter to measure the LED power (P) incident on the solution at the irradiation wavelength λ_{irr}. Photons absorbed (N_{abs}) were calculated from the incident photon flux (I_0) and the solution absorbance (A) at λ_{irr} according to eqs 1 and 2 (P = power in J s^{-1}, E = J photon^{-1} at λ_{irr}, and t = photolysis time in s).

$$I_0 = P/E \tag{1}$$

$$N_{abs} = (1 - 10^{-A})I_0xt \tag{2}$$

The number of molecules reacted ($N_{reacted}$) can be calculated from the absorption changes ($A_0 - A_t$) at monitoring wavelengths where extinction coefficient changes ($\Delta\varepsilon = \varepsilon_0 - \varepsilon_{final}$) and the solution volume had been determined. The quantum yield Φ can thus be determined from eq 3. In practice, Φ values were not determined from single data points but from the slopes of the $N_{reacted}$ versus N_{abs} plots (Figure 10). All quantum yield measurements were corrected for any dark reactions.

$$\Phi = N_{reacted}/N_{abs} \tag{3}$$

DFT Calculations. All DFT and TDDFT computations were performed with *Spartan'14* or *Gaussian'09* software packages at an unrestricted B3LYP/6-31G* (LANL2DZ > Kr) level of theory without symmetry constraints.

■ ASSOCIATED CONTENT

Supporting Information

The Supporting Information is available free of charge on the ACS Publications website at DOI: 10.1021/acs.inorgchem.6b03138.

Additional documentation (4 tables and 20 figures) of the studies described in this manuscript including crystallographic parameters, along with minor modifications of published synthetic procedures used to prepare the compounds described (PDF)

X-ray crystallographic data in CIF format (CIF)

X-ray crystallographic data in CIF format (CIF)

X-ray crystallographic data in CIF format (CIF)

X-ray crystallographic data in CIF format (CIF)

■ AUTHOR INFORMATION

Corresponding Author

*E-mail: ford@chem.ucsb.edu.

ORCID

Peter C. Ford: 0000-0002-5509-9912

Notes

The authors declare no competing financial interest.

■ ACKNOWLEDGMENTS

This work was supported by grants to P.C.F. from the Chemistry Division of the United States National Science Foundation (Grants CHE-1405062 and CHE-1565702). We thank Professor Filippo De Angelis of CNR-ISTM, Perugia, Italy, for his advice on TDDFT computations.

■ REFERENCES

(1) Center for Disease Control, http://www.cdc.gov/niosh/idlh/630080.html.

(2) Sjöstrand, T. Endogenous Formation of Carbon Monoxide in Man Under Normal and Pathological Conditions. *Scand. J. Clin. Lab. Invest.* **1949**, *1*, 201−214; Also. *Nature* **1949**, *164*, 580−581.

(3) Heinemann, S. H.; Hoshi, T.; Westerhausen, M.; Schiller, A. Carbon monoxide − physiology, detection and controlled release. *Chem. Commun.* **2014**, *50*, 3644−3660.

(4) Motterlini, R.; Otterbein, L. E. The therapeutic potential of carbon monoxide. *Nat. Rev. Drug Discovery* **2010**, *9*, 728−743.

(5) Otterbein, L. E. Carbon Monoxide: Innovative Anti-inflammatory Properties of an Age-Old Gas Molecule. *Antioxid. Redox Signaling* **2002**, *4*, 309−319.

(6) Babu, D.; Motterlini, R.; Lefebvre, R. A. CO and CO-releasing molecules (CO-RMs) in acute gastrointestinal inflammation. *Br. J. Pharmocol.* **2015**, *172*, 1557−1573.

(7) Wilkinson, W. J.; Kemp, P. J. Carbon monoxide: an emerging regulator of ion channels. *J. Physiol.* **2011**, *589*, 3055−3062.

(8) Kitagishi, H.; Minegishi, S.; Yumura, A.; Negi, S.; Taketani, S.; Amagase, Y.; Mizukawa, Y.; Urushidani, T.; Sugiura, Y.; Kano, K. Feedback Response to Selective Depletion of Endogenous Carbon Monoxide in the Blood. *J. Am. Chem. Soc.* **2016**, *138*, 5417−5425.

(9) Nassour, I.; Kautza, B.; Rubin, M.; Escobar, D.; Luciano, J.; Loughran, P.; Gomez, H.; Scott, J.; Gallo, D.; Brumfield, J.; Otterbein, L. E.; Zuckerbraun, B. S. Carbon Monoxide Protects Against Hemorrhagic Shock and Resuscitation-induced Microcirculatory and Tissue Injury. *Shock* **2015**, *43*, 166−171.

DOI: 10.1021/acs.inorgchem.6b03138
Inorg. Chem. 2017, 56, 6094−6104

(10) Halilovic, A.; Patil, K. A.; Bellner, L.; Marrazzo, G.; Castellano, K.; Cullaro, G.; Dunn, M. W.; Schwartzman, M. L. Knockdown of Heme Oxygenase-2 Impairs Corneal Epithelial Cell Wound Healing. *J. Cell. Physiol.* **2011**, *226*, 1732−1740.
(11) Otterbein, L. E.; Zuckerbraun, B.; Haga, M.; Liu, F.; Song, R.; Usheva, A.; Stachulak, C.; Bodyak, N.; Smith, R. N.; Csizmadia, E.; Tyagi, S.; Akamatsu, Y.; Flavell, R. J.; Billiar, T. R.; Tzeng, E.; Bach, F. H.; Choi, A. M. K.; Soares, M. P. Carbon monoxide suppresses arteriosclerotic lesions associated with chronic graft rejection and with balloon injury. *Nat. Med.* **2003**, *9*, 183−190.
(12) Ryter, S. W.; Morse, D.; Choi, A. M. K. Carbon monoxide and bilirubin - Potential therapies for pulmonary/vascular injury and disease. *Am. J. Respir. Cell Mol. Biol.* **2007**, *36*, 175−182.
(13) Simpson, P. V.; Nagel, C.; Bruhn, H.; Schatzschneider, U. Antibacterial and Antiparasitic Activity of Manganese(I) Tricarbonyl Complexes with Ketoconazole, Miconazole, and Clotrimazole Ligands. *Organometallics* **2015**, *34*, 3809−3815.
(14) Nobre, L. S.; Jeremias, H.; Romão, C. C.; Saraiva, L. M. Examining the antimicrobial activity and toxicity to animal cells of different types of CO-releasing molecules. *Dalton Trans.* **2016**, *45*, 1455−1466.
(15) Klinger-Strobel, M.; Glaeser, S.; Makarewicz, O.; Wyrwa, R.; Weisser, J.; Pletz, M. W.; Schiller, A. Bactericidal Effect of a Photoresponsive Carbon Monoxide-Releasing Nonwoven against Staphylococcus aureus Biofilms. *Antimicrob. Agents Chemother.* **2016**, *60*, 4037−4046.
(16) Wilson, J. L.; Jesse, H. E.; Poole, R. K.; Davidge, K. S. Antibacterial Effects of Carbon Monoxide. *Curr. Pharm. Biotechnol.* **2012**, *13*, 760−768.
(17) Fukuto, J. M.; Carrington, S. J.; Tantillo, D. J.; Harrison, J. G.; Ignarro, L. J.; Freeman, B. A.; Chen, A.; Wink, D. A. Small Molecule Signaling Agents: The Integrated Chemistry and Biochemistry of Nitrogen Oxides, Oxides of Carbon, Dioxygen, Hydrogen Sulfide, and Their Derived Species. *Chem. Res. Toxicol.* **2012**, *25*, 769−793.
(18) Chance, B.; Erecinska, M.; Wagner, M. Mitochondrial Responses to Carbon Monoxide Toxicity. *Ann. N. Y. Acad. Sci.* **1970**, *174*, 193−204.
(19) Mann, B. E. CO-Releasing Molecules: A Personal View. *Organometallics* **2012**, *31*, 5728−5735.
(20) Romão, C. C.; Blaettler, W. A.; Seixas, J. D.; Bernardes, G. J. L. Developing drug molecules for therapy with carbon monoxide. *Chem. Soc. Rev.* **2012**, *41*, 3571−83.
(21) Schatzschneider, U. Novel lead structures and activation mechanisms for CO-releasing molecules (CORMs). *Br. J. Pharmacol.* **2015**, *172*, 1638−1650.
(22) Romanski, S.; Kraus, B.; Schatzschneider, U.; Neudorfl, J.-M.; Amslinger, S.; Schmalz, H.-G. Acyloxybutadiene Iron Tricarbonyl Complexes as Enzyme-Triggered CO-Releasing Molecules (ET-CORMs). *Angew. Chem., Int. Ed.* **2011**, *50*, 2392−2396.
(23) Fujita, K.; Tanaka, Y.; Sho, T.; Ozeki, S.; Abe, S.; Hikage, T.; Kuchimaru, T.; Kizaka-Kondoh, S.; Ueno, T. Intracellular CO Release from Composite of Ferritin and Ruthenium Carbonyl Complexes. *J. Am. Chem. Soc.* **2014**, *136*, 16902−16908.
(24) Chaves-Ferreira, M.; Albuquerque, I. S.; Matak-Vinkovic, D.; Coelho, A. C.; Carvalho, S. M.; Saraiva, L. M.; Romão, C. C.; Bernardes, G. J. L.Spontaneous CO Release from $Ru^{II}(CO)_2$−Protein Complexes in Aqueous Solution, Cells, and Mice. *Angew. Chem., Int. Ed.* **2015**, *54*, 1172−1175.
(25) Motterlini, R.; Clark, J. E.; Foresti, R.; Sarathchandra, P.; Mann, B. E.; Green, C. J. Carbon Monoxide-Releasing Molecules: Characterization of Biochemical and Vascular Activities. *Circ. Res.* **2002**, *90*, 17e−24e.
(26) Rimmer, R. D.; Richter, H.; Ford, P. C. A Photochemical Precursor for Carbon Monoxide Release in Aerated Aqueous Media. *Inorg. Chem.* **2010**, *49*, 1180−1185.
(27) Schatzschneider, U. PhotoCORMs: Light-triggered release of carbon monoxide from the coordination sphere of transition metal complexes for biological applications. *Inorg. Chim. Acta* **2011**, *374*, 19−23.
(28) Rimmer, R. D.; Pierri, A. E.; Ford, P. C. Photochemically activated carbon monoxide release for biological targets. Toward developing air-stable photoCORMs labilized by visible light. *Coord. Chem. Rev.* **2012**, *256*, 1509−1519.
(29) Pierri, A. E.; Pallaoro, A.; Wu, G.; Ford, P. C. A Luminescent and Biocompatible PhotoCORM. *J. Am. Chem. Soc.* **2012**, *134*, 18197−18200.
(30) Gonzalez, M. A.; Yim, M. A.; Cheng, S.; Moyes, A.; Hobbs, A. J.; Mascharak, P. K. Manganese Carbonyls Bearing Tripodal Polypyridine Ligands as Photoactive Carbon Monoxide-Releasing Molecules. *Inorg. Chem.* **2012**, *51*, 601−608.
(31) Yempally, V.; Kyran, S. J.; Raju, R. K.; Fan, W. Y.; Brothers, E. N.; Darensbourg, D. J.; Bengali, A. A. Thermal and Photochemical Reactivity of Manganese Tricarbonyl and Tetracarbonyl Complexes with a Bulky Diazabutadiene Ligand. *Inorg. Chem.* **2014**, *53*, 4081−4088.
(32) Govender, P.; Pai, S.; Schatzschneider, U.; Smith, G. Next Generation PhotoCORMs: Polynuclear Tricarbonylmanganese(I)-Functionalized Polypyridyl Metallodendrimers. *Inorg. Chem.* **2013**, *52*, 5470−5478.
(33) Bohlender, C.; Gläser, S.; Klein, M.; Weisser, J.; Thein, S.; Neugebauer, U.; Popp, J.; Wyrwa, R.; Schiller, A. Light-triggered CO release from nanoporous non-wovens. *J. Mater. Chem. B* **2014**, *2*, 1454−1463.
(34) Pierri, A. E.; Huang, P.-J.; Garcia, J. V.; Stanfill, J. G.; Chui, M.; Wu, G.; Zheng, N.; Ford, P. C. A photoCORM nanocarrier for CO release using NIR light. *Chem. Commun.* **2015**, *51*, 2072−2075.
(35) Pierri, A. E.; Muizzi, D. A.; Ostrowski, A. D.; Ford, P. C. Photo-controlled release of NO and CO with inorganic and organometallic complexes. *Struct. Bonding (Berlin, Ger.)* **2014**, *165*, 1−45.
(36) Carrington, S. J.; Chakraborty, I.; Bernard, J. M. L.; Mascharak, P. K. A Theranostic Two-Tone Luminescent PhotoCORM Derived from Re(I) and (2-Pyridyl)-benzothiazole: Trackable CO Delivery to Malignant Cells. *Inorg. Chem.* **2016**, *55*, 7852−8.
(37) Mede, R.; Klein, M.; Claus, R. A.; Krieck, S.; Quickert, S.; Goerls, H.; Neugebauer, U.; Schmitt, M.; Gessner, G.; Heinemann, S. H.; Popp, J.; Bauer, M.; Westerhausen, M. CORM-EDE1: A Highly Water-Soluble and Nontoxic Manganese-Based photoCORM with a Biogenic Ligand Sphere. *Inorg. Chem.* **2016**, *55*, 104−113.
(38) König, K. Multiphoton microscopy in life sciences. *J. Microsc.* **2000**, *200*, 83−104.
(39) Peng, P.; Wang, C.; Shi, Z.; Johns, V. K.; Ma, L.; Oyer, J.; Copik, A.; Igarashi, R.; Liao, Y. Visible light activatable organic CO-releasing molecules (PhotoCORMs) that simultaneously generate fluorophores. *Org. Biomol. Chem.* **2013**, *11*, 6671−6674.
(40) Palao, E.; Slanina, T.; Muchova, L.; Solomek, T.; Vitek, L.; Klan, P. Transition-Metal-Free CO-Releasing BODIPY Derivatives Activatable by Visible to NIR Light as Promising Bioactive Molecules. *J. Am. Chem. Soc.* **2016**, *138*, 126−133.
(41) Kottelat, E.; Ruggi, A.; Zobi, F. Red-light activated photo-CORMs of Mn(I) species bearing electron deficient 2,2′-azopyridines. *Dalton Trans.* **2016**, *45*, 6920−6927.
(42) Ford, P. C. Polychromophoric Metal Complexes for Generating the Bioregulatory Agent Nitric Oxide by Single and Two Photon Excitation. *Acc. Chem. Res.* **2008**, *41*, 190−200.
(43) Garcia, J. V.; Zhang, F.; Ford, P. C. Multi-Photon Excitation in Uncaging the Small Molecule Bioregulator Nitric Oxide. *Philos. Trans. R. Soc., A* **2013**, *371*, 20120129.
(44) Wrighton, M. S.; Bredesen, D. Symmetrical cleavage of the metal-metal bond in decacarbonyl-dirhenium(0) by ultraviolet irradiation. *J. Organomet. Chem.* **1973**, *50*, C35−C38.
(45) Morse, D. L.; Wrighton, M. S. Photochemistry of metal-metal bonded complexes. 5. Cleavage of the M-M bond in $(OC)_5M$-$M(CO)_3L$ by irradiation into a low-lying MML charge-transfer band. *J. Am. Chem. Soc.* **1976**, *98*, 3931−3934.
(46) Almond, M. J.; Orrin, R. H. Photo-oxidation of $[Re_2(CO)_{10}]$ in low-temperature matrices containing O_2. *J. Chem. Soc., Dalton Trans.* **1992**, 1229−1234.

DOI: 10.1021/acs.inorgchem.6b03138
Inorg. Chem. 2017, 56, 6094−6104

(47) Dessy, R. E.; Weissman, P. M. Organometallic Electrochemistry. VIII. The Formation of Metal-Metal Bonds. *J. Am. Chem. Soc.* **1966**, *88*, 5124−5129.
(48) Morse, D. L.; Wrighton, M. S. Reaction of pentacarbonylmanganese(-I) and -rhenium(-I) with metal carbonyl halide derivatives. *J. Organomet. Chem.* **1977**, *125*, 71−77.
(49) Staal, L. H.; Van Koten, G.; Vrieze, K. Binuclear metal carbonyl dab complexes: II. The syntheses and coordination properties of $Mn(CO)_5M'(CO)_3DAB$ (M′ = Mn, Re; DAB = 1,4-diazabutadiene). *J. Organomet. Chem.* **1979**, *175*, 73−86.
(50) Male, J. L.; Lindfors, B. E.; Covert, K. J.; Tyler, D. R. The Effect of Radical Size and Mass on the Cage Recombination Efficiency of Photochemically Generated Radical Cage Pairs. *J. Am. Chem. Soc.* **1998**, *120*, 13176−13186.
(51) Oelkers, A. B.; Tyler, D. R. Radical cage effects: A method for measuring recombination efficiencies of secondary geminate radical cage pairs using pump-probe transient absorption methods *Photochem. Photobiol. Sci.* **2008**, *7*, 1386−1390.
(52) Luong, J. C.; Faltynek, R. A.; Wrighton, M. S. Competitive radiative decay and metal-metal bond cleavage from the lowest excited state of triphenyltin- and triphenylgermanium tricarbonyl(1,10-phenanthroline)rhenium. *J. Am. Chem. Soc.* **1979**, *101*, 1597−1598.
(53) McCullen, S. B.; Brown, T. L. Photochemical reaction of decacarbonyldimanganese with pyridine: evidence for a radical pathway. *Inorg. Chem.* **1981**, *20*, 3528−3533.
(54) Kokkes, M. W.; Stufkens, D. J.; Oskam, A. Photochemistry of metal-metal-bonded complexes. 1. MLCT photolysis of (CO)-5MM′(CO)3(.alpha.-diimine) (M, M′ = Mn, Re) in 2-MeTHF between 133 and 230 K. *Inorg. Chem.* **1985**, *24*, 2934−2942.
(55) Greenwood, N. N.; Earnshaw, A. *Chemistry of the Elements*; Pergamon Press: Oxford, U.K., 1993; p 30.
(56) The solubility of O_2 in MeCN at 25 °C has been reported to be 8.1 mM atm^{-1}. Achord, J. M.; Hussey, C. L. Determination of Dissolved Oxygen in Nonaqueous Electrochemical Solvents. *Anal. Chem.* **1980**, *52*, 601−602.
(57) Laine, R. M.; Ford, P. C. Reactivity of Metal Radicals Generated Photochemically. Effects of Solvent and of Trapping Agent Concentrations on Quantum Yields for Photolysis of Hexacarbonylbis-(p-cyclopentadienyl)-ditungsten(I), $[-CpW(CO)_3]_2$. *Inorg. Chem.* **1977**, *16*, 388−391.
(58) Kurtz, D. A.; Dhakal, B.; Hulme, R. J.; Nichol, G. S.; Felton, G. A. N. Correlations between photophysical and electrochemical properties for a series of new Mn carbonyl complexes containing substituted phenanthroline ligands. *Inorg. Chim. Acta* **2015**, *427*, 22−26.
(59) Church, S. P.; Poliakoff, M.; Timney, J. A.; Turner, J. J. Synthesis and characterization of the pentacarbonylmanganese(0) radical, $Mn(CO)_5$, in low-temperature matrixes. *J. Am. Chem. Soc.* **1981**, *103*, 7515−7520.
(60) Church, S. P.; Hermann, H.; Grevels, F.-W.; Schaffner, K. The primary photoproducts of $Mn_2(CO)_{10}$: direct i.r. observation and decay kinetics of $Mn(CO)_5$ and $Mn_2(CO)_9$ in hydrocarbon solution at room temperature. *J. Chem. Soc., Chem. Commun.* **1984**, *12*, 785−786.
(61) Burks, P. T.; Garcia, J. V.; GonzalezIrias, R.; Tillman, J. T.; Niu, M.; Zhang, J. P.; Zhang, F.; Ford, P. C.; Mikhailovsky, A. A. Nitric Oxide Releasing Materials Triggered by Near-Infrared Excitation Through Tissue Filters. *J. Am. Chem. Soc.* **2013**, *135*, 18145−18152.
(62) Timko, B. P.; Arruebo, M.; Shankarappa, S. A.; McAlvin, J. B.; Okonkwo, O. S.; Mizrahi, B.; Stefanescu, C. F.; Gomez, L.; Zhu, J.; Zhu, A.; Santamaria, J.; Langer, R.; Kohane, D. S. Near-infrared−actuated devices for remotely controlled drug delivery. *Proc. Natl. Acad. Sci. U. S. A.* **2014**, *111*, 1349−1354.
(63) Mase, J. D.; Razgoniaev, A. O.; Tschirhart, M. K.; Ostrowski, A. D. Light-controlled release of nitric oxide from solid polymer composite materials using visible and near infra-red light. *PhotoChem. Photobiol. Sci.* **2015**, *14*, 775−785.
(64) Sugahara, K. N.; Teesalu, T.; Karmali, P. P.; Kotamraju, V. R.; Agemy, L.; Girard, O. M.; Hanahan, D.; Mattrey, R. F.; Ruoslahti, E. Tissue-Penetrating Delivery of Compounds and Nanoparticles into Tumors. *Cancer Cell* **2009**, *16*, 510−520.
(65) Chung, E. J.; Cheng, Y.; Morshed, R.; Nord, K.; Han, Y.; Wegscheid, M. L.; Auffinger, B.; Wainwright, D. A.; Lesniak, M. S.; Tirrell, M. V. Fibrin-binding, peptide amphiphile micelles for targeting glioblastoma. *Biomaterials* **2014**, *35*, 1249−1256.
(66) Fieldhouse, S. A.; Fullam, B. W.; Neilson, G. W.; Symons, M. C. R. Reaction of metal carbonyls with oxygen. *J. Chem. Soc., Dalton Trans.* **1974**, 567−569.
(67) Mach, K.; Nováková, J.; Raynor, J. B. Electron spin resonance spectroscopy of $Mn(CO)_5$· radicals generated in the gas phase thermolysis of $Mn_2(CO)_{10}$. *J. Organomet. Chem.* **1992**, *439*, 341−345.
(68) Lindsell, W. E.; Preston, P. N. Electron spin resonance investigations of the photo-oxidation of decacarbonyldimanganese and related complexes. *J. Chem. Soc., Dalton Trans.* **1979**, *6*, 1105−1108.
(69) Levy, E. S.; Morales, D. P.; Garcia, J. V.; Reich, N. O.; Ford, P. C. Near-IR mediated intracellular uncaging of NO from cell targeted hollow gold nanoparticles. *Chem. Commun.* **2015**, *51*, 17692−17695.
(70) Kokkes, M. W.; Snoeck, T. L.; Stufkens, D. J.; Oskam, A.; Cristophersen, M.; Stam, C. H. Structural and spectroscopic properties of $[(CO)_5MM'(CO)_3(R\text{-}DAB)]$ (M,M′=Mn,Re; R-DAB = 1,4-diaza-1,3-butadiene complexes. X-ray structure of $[(CO)_5ReMn(CO)_3$-(i-Pr-DAB)] and infrared and resonance Raman spectra of $[(CO)_5MM'(CO)_3(R\text{-}DAB)]$. *J. Mol. Struct.* **1985**, *131*, 11−29.
(71) Van Outersterp, J. W. M.; Hartl, F.; Stufkens, D. J. Variable Temperature IR Spectroelectrochemical Investigation of the Stability of the Metal-Metal-Bonded Radical Anions $[(CO)_5MnRe(CO)_3(L)]$.bul.- (L = 2,2′-Bipyridine (BPY), 2,2′-Bipyrimidine (BPYM), 2,3-Bis(2-pyridyl)pyrazine (DPP)) and $[(CO)_5MnRe(CO)_3(L)Re(Br)(CO)_3]$.bul.- (L = BPYM, DPP) Controlled by the Lowest.pi. (.alpha.-Diimine) Orbital Energy. *Organometallics* **1995**, *14*, 3303−3310.

DOI: 10.1021/acs.inorgchem.6b03138
Inorg. Chem. 2017, 56, 6094−6104